Urban Climate 24 (2018) 485–502

Contents lists available at ScienceDirect

Urban Climate

journal homepage: http://www.elsevier.com/locate/uclim

Investigating the relationship between local climate zone and land surface temperature using an improved WUDAPT methodology – A case study of Yangtze River Delta, China

Meng Cai [a], Chao Ren [a,b,c,*], Yong Xu [a], Kevin Ka-Lun Lau [a,c,d], Ran Wang [b]

[a] Institute of Future Cities, The Chinese University of Hong Kong, Hong Kong
[b] School of Architecture, The Chinese University of Hong Kong, Hong Kong
[c] Institute of Energy, Environment and Sustainability. The Chinese University of Hong Kong, Hong Kong
[d] Institute of Aging, The Chinese University of Hong Kong, Hong Kong

ARTICLE INFO

Article history:
Received 27 February 2017
Received in revised form 22 May 2017
Accepted 24 May 2017

Keywords:
Local climate zone
Land surface temperature
WUDAPT
Megaregion
Aster

ABSTRACT

The concept of Local Climate Zone (LCZ) was developed to quantify the relationship between urban morphology and urban heat island (UHI) phenomenon. Each LCZ is supposed to represent homogeneous air temperature. However, there is inadequate data for verifying the air temperature differences between LCZ classes. Therefore, it is necessary to utilize alternative temperature data which allow more comprehensive assessment of the effect of LCZ on local climatic conditions. Land surface temperature (LST) acquired from satellite images can be used to establish the relationship between LST and LCZ by providing continuous data on surface temperature. This paper aims to investigate how LST represents the UHI intensity determined by using an improved method of the World Urban Database and Portal Tool (WUDAPT) to develop the LCZ map of the Yangtze River Delta (YRD) megaregion. The results show that LST in different YRD cities is generally consistent with the LCZ classes with higher LST observed in built-up LCZ classes. The diverse urban morphology and temporal vegetation variation are likely the reasons to inconsistencies in LCZ 9, and LCZ A to D. Findings of this paper provide a better understanding of how urban morphology affects local climate and more accurate delineation of LCZ classes.

* Corresponding author at: Room 505, School of Architecture, The Chinese University of Hong Kong, Shatin, N.T., Hong Kong.
E-mail address: renchao@cuhk.edu.hk (C. Ren)

http://dx.doi.org/10.1016/j.uclim.2017.05.010
2212-0955

1. Introduction

Urbanization in China has reached an unprecedented level with 54.77% of the population living in cities in 2014 (National Bureau of Statistics of China, 2014). With continuous urbanization and the increasing communications between different metropolitan cities, the idea of megaregions was introduced as a new framework for national policy of spatial development (The state council of People's Republic of China, 2016). There are ten megaregions in China with the Pearl River Delta, the Yangtze River Delta (YRD), and the Capital Region as three leading megaregions. Although these three megaregions occupy 1.6% of the total area of China, 10.6% of the total population in China reside in these three megaregions (Amekudzi et al., 2012). Such a high population density results in enormous pressure on the urban systems and challenges to the sustainable urban development of the urban agglomerations.

Urban development converts natural landscape into artificial constructions and pavements, resulting in altered climatic conditions in urban areas and the formation of urban heat island (UHI) phenomenon (Oke, 1982, 1987). The concept of Local Climate Zone (LCZ) was developed to quantify the relationship between urban morphology and UHI phenomenon (Stewart and Oke, 2012). It provides a standardized framework to characterize cities according to the surface properties. Each LCZ class is assumed to be homogeneous in terms of surface properties and the effect on air temperature. One of the major advantages of the LCZ classification system is the new perspective of defining UHI by using the temperature differences among LCZ classes rather than the traditional urban-rural difference. It therefore emphasizes the importance of intra-urban temperature comparison to analyze the influence of heterogeneous urban morphology on the formation of local climate.

For the nature of LCZ classification, air temperature is the most suitable meteorological parameter for analyzing the temperature differences among LCZ classes. However, the coverage of ground-level, observational meteorological stations is generally limited, resulting in poor spatial resolution for verifying the differences in air temperature between LCZ classes. As such, alternative temperature data is necessary for more comprehensive assessment of the effect of urban morphology on local climatic conditions. Satellite images provide continuous coverage, high integrity and real-time data acquisition over large areas (Voogt and Oke, 2003). In addition, satellite images acquired during night-time were found to have stronger relationship between land surface and the adjacent air (Stoll and Brazel, 1992) so they provide a representation of air temperature sufficient for UHI studies at city scale (The state council of People's Republic of China, 2016). As night-time temperature increases at a higher rate than daytime temperature in urban areas due to UHI phenomenon (Schrijvers et al., 2015), LST derived from night-time satellite imagery is a suitable alternative as an indicator of urban heat island.

This paper aims to determine the relationship between LST and LCZ classes with the YRD megaregion selected as a case study. Night-time Aster satellite images of Shanghai and Hangzhou were used to investigate LST from the YRD megaregion, which were subsequently classified to show the surface UHI intensity. An improved method of the World Urban Database and Portal Tool (WUDAPT) was also used to develop the LCZ map of the YRD megaregion. Air temperature data from weather observational stations was used to test against the LST pattern of LCZ classes. LST of different LCZ classes can therefore be characterized in order to inform urban climate researchers and urban planners about the influence of LCZ on local climate, leading to more sustainable urban planning in megaregions in China.

2. Materials and methodology

2.1. Study area: Yangtze River Delta

The YRD region is composed of the territory of Shanghai, southern Jiangsu Province and northern Zhejiang Province (Fig. 1). The terrain of this region is generally flat and low-lying floodplain with some hilly areas located in the south of Hangzhou. The YRD region has a subtropical monsoon climate with annual mean temperature of 15–16 °C and annual precipitation of 1000–1400 mm. Rapid urbanization in this region has given rise to one of the largest megalopolis in the world, covering an area of 99,600 km^2 and home to over the 83-million urban population (National Development and Reform Commission, 2016). This region is selected in the present paper due to the similar geographic characteristics and urban morphology of the YRD cities.

Fig. 1. Location of the study area.

Two typical cities in the YRD megaregion under rapid urban development were selected as case studies in the present paper, namely Shanghai and Hangzhou. Shanghai is located in the centre of the alluvial terrace of the Yangtze River delta. It has the highest population density in China and is one of the most vigorous economic zones in the world (Shanghai Municipal Statistics Bureau, 2011). It is divided into 18 county-level

divisions with nine districts in the city core collectively identified as urban areas. Hangzhou is the capital of the Zhejiang Province and has the highest population in the province. It is located in the southern part of the YRD and now one of China's most prosperous major cities. Hangzhou municipality area includes nine urban districts, two county-level cities and two counties.

Previous studies showed that there is significant UHI phenomenon in the YRD region, characterized by more hot days, higher maximum air temperature and longer duration of high temperature in urban areas than outer suburbs and peri-urban areas (Wang and Zheng, 2013; Zhang et al., 2013). UHI intensity in YRD region reaches 4.7 °C (Dong et al., 2014) and the areas experiencing intense UHI have rapidly expanded. In particular, the average UHI intensity in Shanghai reaches 2.4 °C in summer (Ding et al., 2014) while the maximum UHI intensity reaches 5.6 °C in Hangzhou (Wang and Liu, 1982).

2.2. Data

Landsat 8 level 1 images of the YRD region with a horizontal resolution of 30 m were downloaded from the United States Geological Survey Landsat Data Access Portal. Only 10 Landsat images were selected due to the presence of clouds and their shadow which causes misclassification and false detection of land cover (Zhu and Woodcock, 2012). Therefore, satellite images from August to October were preferred due to the less cloud coverage, leading to more intensified UHI phenomenon (Dong et al., 2014).

Night-time Aster images were also acquired from the National Aeronautics and Space Administration in the present paper since they can better represent the temperature pattern of the YRD region (Table 1) (Nichol and To, 2012). Average air temperature on Sept. 1, 2015 from 28 open available national weather observational stations in the YRD region was also used to validate the temperature pattern of LCZ. Air temperature on Aug. 23, 2015 was not selected as it was rainy and may not present the temperature pattern properly on this date.

2.3. LCZ mapping and validation

2.3.1. LCZ mapping method

LCZ classification generally requires detailed urban morphological data in order to classify the city according to its surface characteristics. However, such data are usually unavailable due to technological limitations and government policies. The WUDAPT methodology was developed to be part of a global protocol to derive information about form and function of cities. It was designed according to the requirements of universality, free availability of data and software, objectivity, computational cost, and convenient application. A standard workflow was therefore developed that uses free multi-temporal Landsat imagery, training data digitized in a Google Earth template and a Random Forest classifier. The algorithm is implemented as a tool in SAGA GIS, an open source software (Bechtel et al., 2015), which consists of three major steps: a) pre-processing of Landsat images; b) digitalization of training samples in Google Earth; c) classification in SAGA GIS.

The existing WUDAPT methodology is at city scale. However, the process of selecting training samples and preprocessing satellite images is very time-consuming for the classification of individual city, especially for large regions that cover a number of cities. An improved WUDAPT method was proposed to generate regional LCZ map, which is designed to classify a large region in the first place and extract the cities in the region

Table 1
Satellite images acquired in the present paper.

Satellite image	Entity ID	Acquisition date	Satellite image	Entity ID	Acquisition date
Landsat 8	LC81200392013287	2013/10/15	Landsat 8	LC81180392015215	2015/08/04
	LC81200402013287	2013/10/15		LC81190402015215	2015/08/04
	LC81190372014075	2014/03/17		LC81190392015286	2015/10/14
	LC81190382014075	2014/03/17		LC81190402015286	2015/10/14
	LC81200372014274	2014/10/02			
	LC81200382014322	2014/11/19	Aster	AST_L1A.003:2185968921	2015/08/23
	LC81180382015215	2015/08/04		AST_L1A.003:2187758991	2015/09/01

correspondingly, instead of classifying each city individually. It applies atmospheric correction to the satellite images of the region in order to eliminate the atmospheric difference among the images, which can improve the image quality in comparison with the existing method. LCZ maps, with the efficiency and accuracy of classification significantly improved, can therefore be provided to researchers and potential users at both regional and city scales. This methodology has been applied to develop LCZ maps for 57 Chinese cities and regions (Cai et al., 2016; Ren et al., 2016a).

In the present paper, 10 Landsat images covering the entire YRD megaregion were selected for the classification. Training samples of the six YRD cities were produced using the improved methodology which contains four major steps as below:

1. *Preprocessing of the Landsat data:* Seamless mosaic and atmospheric correction were applied to the 10 Landsat images to eliminate the atmospheric difference and subsequently combined into one image. The image was then resampled from 30 to 100 m to get a representation of the spectral signal of local-scale urban structures rather than smaller objects.
2. *Digitization of training areas in Google Earth:* Representative areas of each LCZ class were selected by polygons as training samples (Table 2). Each LCZ class contains about 50 polygons. The training samples of six typical YRD cities including Shanghai, Hangzhou, Nanjing, Wuxi, Suzhou, and Yangzhou were used for subsequent classification.

In particular, compact low-rise (LCZ 3), open low-rise (LCZ 6) and Lightweight low-rise (LCZ7) may appear similar in Google earth images as they are all low-rise buildings. The major differences are green space and construction materials. Low-rise buildings with abundance of greenery will be chosen as LCZ 6. Google Street view can provide more detailed and clearer images that can present their building materials to distinguish LCZ 3 and LCZ 7. Low-rise buildings constructed by Lightweight construction materials (e.g., wood, thatch, corrugated metal) will be selected as LCZ 7.

Also, The Landsat images have been acquired in different years (2013–2015) and many land uses could have been changed meanwhile due to rapid urbanization. In order to eliminate the inconsistency of the land covers in different years, places that are likely to change such as construction sites, vacant development areas and bare land will not be selected as training samples.

3. *Classification in SAGA GIS:* The preprocessed Landsat images and the selected training areas of the whole YRD megaregion were inputted into SAGA GIS. The LCZ classification of study areas was then calculated and conducted by random forest classifiers according to the similarity between the training samples and the rest of study areas. The LCZ map of the YRD megaregion was therefore generated.
4. *Extraction of the cities in the YRD region:* The boundaries of the municipalities were used to separately extract the municipalities in the YRD region. The LCZ maps of the 16 municipalities were generated by using the method in Step 3.

2.3.2. Accuracy assessment

Accuracy assessment was conducted to evaluate the performance of the random forest classifier and the accuracy of LCZ classification in the YRD megaregion. Random forest (Liaw and Wiener, 2002) was chosen as the classifier for the WUDAPT methodology due to its high accuracy and computational performance. Moreover, it does not require urban morphology parameters that vary across LCZ classes in a city, which considerably simplifies the workflow. In addition, random forest provides an unbiased error estimate without requiring additional testing data (Bechtel et al., 2015).

A new set of samples for all LCZs was randomly collected as reference data to estimate the classification error. In order to maintain the objectivity, the number of new samples for each LCZ class was set at 0.5% of the number of each LCZ class previously developed. By comparing the developed LCZ classes with the reference data, the assessment results were obtained and summarized in a confusion matrix of which the degree of confusion between the resultant classifications and the ground truth can be calculated.

2.4. LST retrieval

The present study employs single channel algorithm to retrieve LST from remote sensing data because of its relatively simple data requirements and high accuracy (Jiménez-Muñoz, 2003). It is a commonly used

Table 2
Snapshots of different LCZ classes in the YRD megaregion from Google Earth.

LCZ 1: Compact high-rise	**LCZ 2: Compact mid-rise**	**LCZ 3: Compact low-rise**
• Tightly packed buildings with more than 10 stories • Little or no green space • Built by concrete, steel, stone and glass $,100\%) = "fixed_3 10_t 1"$	• Tightly packed buildings with three to nine stories • Little or no green space • Built by stone, brick, tile and concrete $,100\%) = "fixed_3 10_t 2"$	• Tightly packed buildings with one to three stories • Little or no green space • Built by concrete, steel, stone and glass $,100\%) = "fixed_3 10_t 3"$
LCZ 4: Open high-rise	**LCZ 5: Open mid-rise**	**LCZ 6: Open low-rise**
• Openly arranged buildings with more than 10 stories • Abundance green space • Built by concrete, steel, stone and glass $,100\%) = "fixed_3 10_t 4"$	• Openly arranged buildings with three to nine stories • Abundance of green space • Built by concrete, steel and glass $,100\%) = "fixed_3 10_t 5"$	• Openly arranged buildings with one to three stories • Abundance of green space • Built by wood, brick, tile and concrete $,100\%) = "fixed_3 10_t 6"$
LCZ 7: Lightweight low-rise	**LCZ 8: Large low-rise**	**LCZ 9: Sparsely built**
• Lightweight building materials with one to two stories • Few or no trees • Land cover is hard-packed $,100\%) = "fixed_3 10_t 7"$	• Large, openly arranged buildings with one to three stories • Few green space • Land cover is mostly paved $,100\%) = "fixed_3 10_t 8"$	• Sparse arrangement of small or medium-sized buildings in natural setting • Abundance of pervious cover $,100\%) = "fixed_3 10_t 9"$
LCZ 10: Heavy industry	**LCZ A: Dense trees**	**LCZ B: Scattered trees**
• Low-rise and mid-rise industrial structures (towers, tanks, stacks) • Few or no trees $,100\%) = "fixed_3 10_t 10"$	• Heavily wooded landscape of deciduous and/or evergreen trees $,100\%) = "fixed_3 10_t 11"$	• Lightly wooded landscape of deciduous and/or evergreen trees $,100\%) = "fixed_3 10_t 12"$
LCZ C: Bush, scrub	**LCZ D: Low plants**	**LCZ E: Bare rock or paved**
• Open arrangement of bushes, shrubs and short, woody trees $,100\%) = "fixed_3 10_t 13"$	• Grass or herbaceous plants/crops $,100\%) = "fixed_3 10_t 14"$	• Rock or paved cover $,100\%) = "fixed_3 10_t 15"$
LCZ F: Bare soil or sand	**LCZ G: Water**	
• Soil or sand cover $,100\%) = "fixed_3 10_t 16"$	• Large, open water bodies $,100\%) = "fixed_3 10_t 17"$	

approach to estimate LST based on thermal-infrared remote sensing image data (Jiménez-Muñoz et al., 2006). The single channel algorithm only requires one thermal-infrared channel and uses the same equation and coefficients for different sensors while the split-window algorithm requires simultaneous data from at least two sensor channels (Wan, 1996). In addition, it only requires atmospheric moisture content and land surface emissivity as parameters, making it widely applied in UHI studies.

Two night-time Aster Level 1B images with 90 m horizontal resolution were used to acquire LST for Shanghai and Hangzhou. Band 13 of the Aster images was selected for calculation using four major steps:

1. The digital number values of Band 13 of the Aster images were converted to radiance (L_{sen}) using the unit conversion coefficient of 5.69×10^{-3} (ERSDAC, 2010);

2. Black body temperature was computed using Eq. (1) derived from the inversion of Plank's function (Sobrino, 2010):

$$T_{sen} = \frac{K_2}{\ln\left(\frac{K_1}{L_{sen}} + 1\right)} \tag{1}$$

$$\gamma \approx \frac{{T_{sen}}^2}{K_2 L_{sen}} \tag{2}$$

$$\delta \approx T_{sen} - \frac{{T_{sen}}^2}{K_2} \tag{3}$$

where K_1 and K_2 are radiation constants. For Band 13, $K_1 = 865.25\ W \cdot m^{-2} \cdot sr^{-1} \cdot \mu m^{-1}$, $K_2 = 1349.82$ K. γ and δ are two parameters dependent on the Planck's function.

3. Surface emissivity (ε) was retrieved using the Normalized Difference Vegetation Index (NDVI; Jiménez-Muñoz et al., 2006). The surface emissivity for Band 13 was calculated using Eq. (5):

$$P_V = \left(\frac{NDVI - NDVI_S}{NDVI_V - NDVI_S}\right)^2 \tag{4}$$

$$\varepsilon = 0.986 + 0.022 P_V \tag{5}$$

where $NDVI_V$ and $NDVI_S$ are the NDVI values of full vegetation cover ($P_V = 1$) and bare soil ($P_V = 0$) respectively.

4. LST was then retrieved using the following general equation (Jiménez-Muñoz, 2003):

$$T_s = \gamma\left[\frac{1}{\varepsilon}(\psi_1 L_{sen} + \psi_2) + \psi_3\right] + \delta \tag{6}$$

where T_S and ε is the LST and surface emissivity respectively, and ψ_1, ψ_2 and ψ_3 are referred to as atmospheric functions.

2.5. Surface UHI intensity classification

The surface UHI, which can be represented by LST (Schrijvers et al., 2015), in Shanghai and Hangzhou is classified into five levels according to the standard deviation from the mean value (Table 3; Zhang et al., 2013). The advantage of using mean value and standard deviation is that the spatial differentials of LST can be revealed regardless of the temporal variation of the actual LST values.

Table 3
Threshold values for LST classification. μ and SD are the mean value and the standard deviation of LST respectively (Chen et al., 2016; Zhang et al., 2013).

LST category	Range
Very low	$T_S < \mu - 1$ SD
Low	$\mu - 1$ SD $\le T_S < \mu -$ SD/3
Medium	$\mu -$ SD/3 $\le T_S < \mu +$ SD/3
High	$\mu +$ SD/3 $< T_S < \mu + 1$ SD
Very high	$T_S \ge \mu + 1$ SD

2.6. Testing against LST with air temperature

Buffer analysis was applied to the 28 observational stations to determine their most representative LCZ and 300-meter buffer is most suitable for air temperature analysis (Stewart, 2011). The majority LCZ class in the buffer area of each station was determined as the most representative of the station. Afterwards, the average air temperature of the weather observational stations representing same LCZ class was calculated.

3. Results and analysis

3.1. LCZ maps of the YRD megaregion

Fig. 2 is the LCZ map of the YRD megaregion produced by the improved WUDAPT method. It captures the morphological characteristics of both rural and urban areas and detects the spatial pattern of potential UHI phenomenon. As shown in Fig. 2, the vegetation in the central and northern YRD is dominated by farmland (LCZ D) while the southern and southwestern parts of the YRD megaregion are mainly mixed forestland. The vegetation pattern is consistent with the geographic characteristics of the YRD with low-lying alluvial floodplain in the northern half of the YRD and mountainous terrain in the southwest.

Shanghai has the largest urban areas among all the YRD cities according to the LCZ map. The urban areas have expanded to adjacent cities, namely Suzhou, Wuxi and Changzhou. These four cities have been integrated into a large city group with no obvious non-urban areas between the cities. Large urban areas are also identified in the two sub-provincial-level cities, Hangzhou and Nanjing. There are also many isolated urban settlements in the northern part of YRD, which are mainly suburbs and prefecture-level cities that are possible heat sources of the YRD region.

Downtown areas of Shanghai Municipality, especially in city centre where the CBDs and commercial areas are situated, are extremely dense and compact so they are mainly classified into the LCZ 1–4 which are potentially of high UHI intensity. Compact urban land cover is also found in the northern suburbs. Also, the LCZ map also detects LCZ 10 (heavy industry) in Baoshan district in the north and Minhang district in the middle of Shanghai that are sources of anthropogenic heat.

The LCZ map of Hangzhou indicates that LCZ A (dense trees) occupies most of rural areas in the mountain region. Urban settlements are concentrated in the northeastern downtown area. They are not as dense as Shanghai since mainly LCZ 2–5 are found in this region where the UHI phenomenon possibly occurs. In addition, the continuously connected downtown area and suburbs indicate potential aggregation of the UHI phenomenon in Hangzhou. The rest of the counties and county-level cities are mostly classified into LCZ 3 (compact low-rise).

3.2. Validation and accuracy assessment

The confusion matrices present the user and producer accuracy of each LCZ class as well as the overall accuracy and the Kappa coefficient (Tables 4–6). The overall accuracy is 66.53% and the Kappa coefficient is 0.64 for the LCZ map of the YRD region. The overall accuracy of the LCZ maps of Shanghai and Hangzhou are 76.3% and 75.5% respectively. They show acceptable accuracy for the classification at both regional and city scales and can be used for further studies. The improved methodology is more capable of differentiating land cover characteristics due to its higher accuracy. Moreover, the LCZ map of Shanghai exhibits the lowest accuracy for built-up areas (30.3%) since the urban areas in Shanghai are compact with mixed LCZ types.

There are also variations in the accuracy of different LCZ classes. In particular, LCZ 1 and 2 show relatively poor classification results with the producer accuracy lower than 50% in the LCZ maps of the YRD region and Shanghai whereas the LCZ map of Hangzhou has low producer accuracy in LCZ 1 and 3. The misclassification of LCZ 1–3 is likely due to the limited information of Landsat images about building height.

In addition, there are misclassifications in vegetation cover like LCZ B and C since it is difficult for the random forest classifier to distinguish vegetation with various height and density. It is also because the satellite imagery does not contain sufficient information about the height and density of vegetation. On the other hand, the misclassification is resulted from the inconsistent dates of the images obtained from Google Earth and Landsat data since the density and height of vegetation may vary across different seasons. Therefore, multi-temporal Landsat images are required to provide more accurate results.

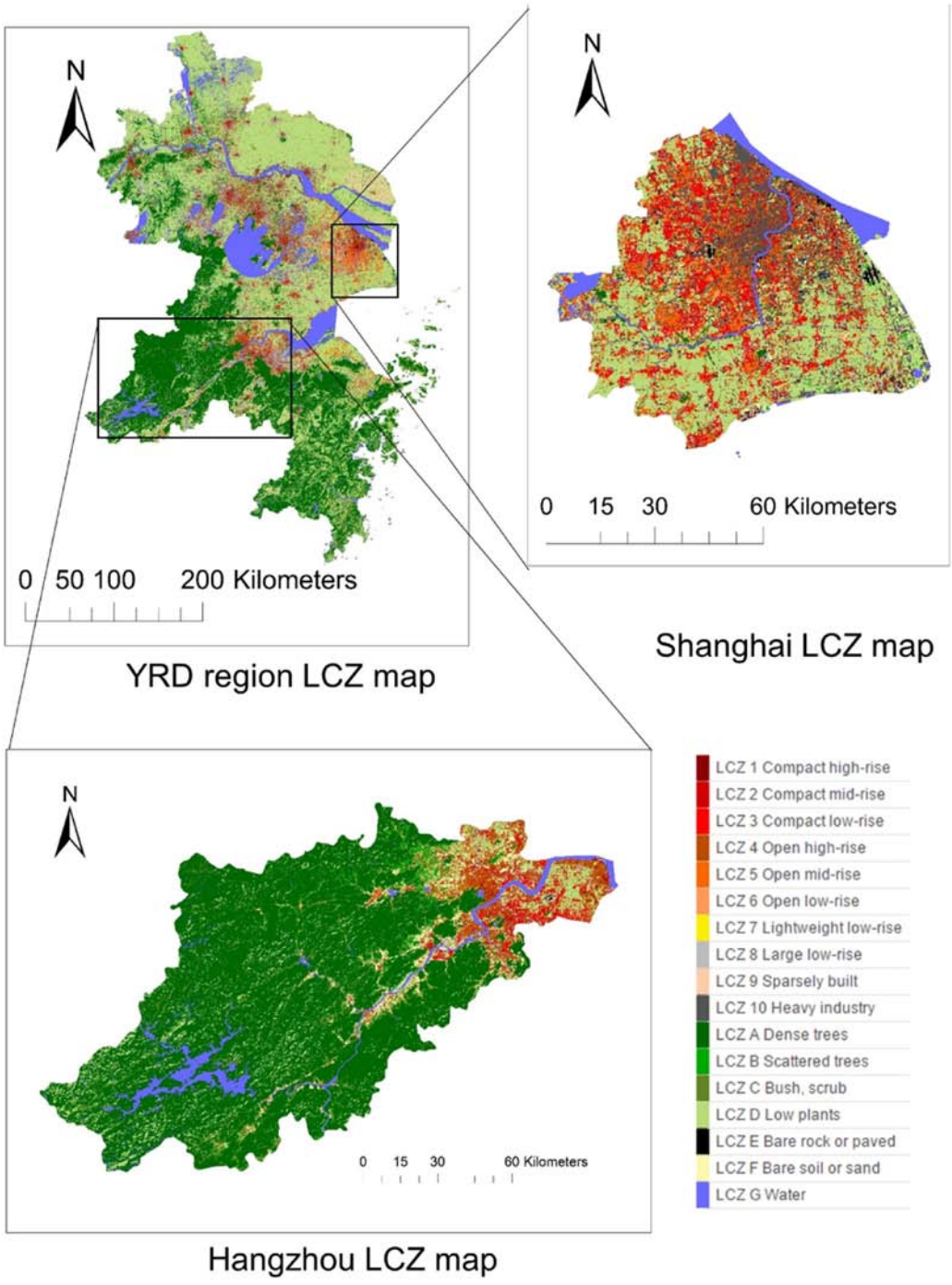

Fig. 2. LCZ maps in the YRD megaregion. Insert.

Table 4
Confusion matrix of the LCZ map of the YRD region.

LCZ	1	2	3	4	5	6	7	8	9	10	A	B	C	D	E	F	G	No. classified pixels	User accuracy
1	15	0	0	0	0	0	0	0	0	0	0	0	0	0	0	0	1	16	93.75%
2	0	34	0	0	0	0	2	0	0	0	0	0	0	0	0	0	0	36	94.44%
3	0	7	43	2	6	0	5	0	0	0	0	0	0	0	0	0	0	63	68.25%
4	11	14	1	46	14	3	1	0	11	7	0	5	1	0	7	13	2	136	33.82%
5	3	3	0	6	55	0	0	1	0	2	0	0	0	0	0	0	0	70	78.57%
6	0	1	1	0	0	12	0	1	2	1	0	2	1	0	1	0	0	22	54.55%
7	0	0	2	0	0	0	2	0	0	0	0	0	0	0	0	0	0	4	50.00%
8	2	1	0	0	0	0	0	87	0	0	0	2	0	0	5	0	0	97	89.69%
9	0	0	0	0	0	0	0	0	4	0	0	0	0	0	0	0	0	4	100.00%
10	0	16	1	11	5	1	0	0	0	43	0	1	0	0	7	5	0	90	47.78%
A	0	1	3	0	1	17	4	11	3	1	98	3	0	4	0	9	0	155	63.23%
B	0	0	0	0	0	0	0	0	0	0	0	8	0	0	0	2	0	10	80.00%
C	0	0	0	0	0	0	0	0	0	0	0	0	4	0	0	0	0	4	100.00%
D	4	0	0	2	3	1	0	3	20	7	8	3	7	48	0	6	0	112	42.86%
E	0	0	0	0	0	0	2	0	0	2	0	1	0	0	78	0	0	83	93.98%
F	0	0	0	0	0	0	0	0	0	0	0	0	0	0	1	11	0	12	91.67%
G	0	0	0	0	0	1	0	0	0	0	0	0	0	0	0	0	62	63	98.41%
No. ground truth pixels	35	77	51	67	84	35	16	103	40	63	106	25	13	52	99	46	65	977	
Producer accuracy	42.86%	44.16%	84.31%	68.66%	65.48%	34.29%	12.50%	84.47%	10.00%	68.25%	92.45%	32.00%	30.77%	92.31%	78.79%	23.91%	95.38%		
Overall accuracy	66.53%	Built-ups accuracy				54.65%					Land coverings accuracy				62.80%				
Kappa	0.6373																		

Table 5
Confusion matrix of the LCZ map of Shanghai.

LCZ	1	2	3	4	5	6	7	8	9	10	A	B	C	D	E	F	G	No. classified pixels	User accuracy
1	1	0	0	5	1	0	1	1	0	0	0	0	0	0	0	0	0	9	11.11%
2	1	4	5	4	1	0	3	0	0	0	0	0	0	0	0	0	0	18	22.22%
3	0	5	42	5	0	2	2	5	0	2	0	0	0	1	6	0	0	70	60.00%
4	1	1	0	30	8	7	0	0	0	0	2	0	0	16	0	0	0	65	46.15%
5	0	4	2	4	4	3	2	1	0	0	0	0	0	5	1	0	0	26	15.38%
6	0	1	0	4	6	35	1	0	0	0	2	0	0	21	0	2	0	72	48.61%
7	1	3	6	0	0	2	8	0	0	0	0	0	0	4	0	0	0	24	33.33%
8	0	0	5	1	0	1	0	24	0	1	0	0	0	0	2	1	0	35	68.57%
9	0	0	0	0	0	0	0	0	2	0	0	0	0	0	0	0	0	2	100.00%
10	4	4	7	24	3	4	2	3	0	2	0	1	0	66	1	5	2	128	1.56%
A	0	0	0	2	0	0	1	0	0	0	14	1	0	0	0	0	0	18	77.78%
B	0	0	0	0	0	3	0	0	0	0	0	1	0	7	0	1	0	12	8.33%
C	0	0	0	0	0	1	0	0	0	0	0	2	3	11	0	2	0	19	15.79%
D	0	0	0	2	0	1	1	0	2	1	0	0	2	295	1	0	0	305	96.72%
E	0	0	7	1	0	0	0	12	0	0	0	0	0	3	32	2	0	57	56.14%
F	0	0	0	0	0	0	0	0	1	0	1	0	0	77	0	4	0	83	4.82%
G	0	0	0	0	1	0	0	0	0	0	0	0	0	4	0		939	944	99.47%
No. ground truth pixels	8	22	74	82	24	59	21	46	5	6	19	5	5	510	43	17	941	1887	
Producer accuracy	12.50%	18.18%	56.76%	36.59%	16.67%	59.32%	38.10%	52.17%	40.00%	33.33%	73.68%	20.00%	60.00%	57.84%	74.42%	23.53%	99.79%		
Overall accuracy	76.31%	Built-ups accuracy				31.34%					Land coverings accuracy				81.73%				
Kappa	0.6618																		

Table 6
Confusion matrix of the LCZ map of Hangzhou.

LCZ	1	2	3	4	5	6	7	8	9	10	A	B	C	D	E	F	G	No. classified pixels	User accuracy
1	11	1	0	7	0	0	0	0	0	0	0	0	0	0	0	0	1	20	55.00%
2	2	19	6	0	10	1	0	3	1	1	0	0	0	1	0	0	0	44	43.18%
3	0	1	8	0	1	0	1	18	0	0	0	0	0	0	1	0	0	30	26.67%
4	23	3	0	49	0	2	2	0	0	0	0	0	0	3	0	0	4	86	56.98%
5	0	1	0	0	15	0	2	0	0	0	0	1	0	0	0	0	0	19	78.95%
6	0	0	1	3	2	22	12	0	3	0	0	0	0	1	0	0	2	46	47.83%
7	0	0	5	0	0	0	15	3	0	0	0	0	0	0	0	0	0	23	65.22%
8	0	1	0	2	1	0	0	12	0	0	0	0	0	0	4	3	0	23	52.17%
9	0	0	0	2	0	2	0	0	5	0	0	0	0	19	0	0	1	29	17.24%
10	0	1	1	1	0	0	0	0	0	5	0	0	0	0	0	0	0	8	62.50%
A	0	0	0	0	0	0	0	0	0	0	162	3	0	0	0	0	0	165	98.18%
B	0	0	0	0	0	3	0	0	0	0	2	31	0	0	0	0	0	36	86.11%
C	0	0	0	0	0	0	0	0	0	0	0	2	14	0	0	0	0	16	87.50%
D	0	0	1	2	0	2	7	0	4	0	1	6	0	122	0	5	2	152	80.26%
E	0	0	0	0	0	0	0	0	0	0	0	0	0	0	45	0	0	45	100.00%
F	0	0	0	0	1	0	3	0	0	0	0	4	0	31	1	10	0	50	20.00%
G	0	0	0	0	0	0	0	0	0	0	0	0	0	0	0	0	216	216	100.00%
No. ground truth pixels	36	27	22	66	30	32	42	36	13	6	165	47	14	177	51	18	226	1008	
Producer accuracy	30.56%	70.37%	36.36%	74.24%	50.00%	68.75%	35.71%	33.33%	38.46%	83.33%	98.18%	65.96%	100%	68.93%	88.24%	55.56%	95.58%		
Overall accuracy	75.50%	Built-ups accuracy				45.87%					Land coverings accuracy				83.22%				
Kappa	0.7220																		

3.3. Classification of surface UHI intensity

The surface UHI of Shanghai and Hangzhou were classified according to Table 3. Fig. 3 shows the spatial pattern of surface UHI classified in Shanghai and Hangzhou based on the LST acquired from night-time Aster thermal images. In Shanghai, the surface UHI intensity reaches up to 4.2 °C in downtown areas in the centre and northern part of Shanghai. High LST was extensive found in the southern suburbs while scattered, extremely high LST values were observed outside city centre due to the presence of point sources like the factories in the north of Baoshan and the south of Minghang. It is also notable that the distribution of high LST is dominant in the city.

Surface UHI is more prominent in Hangzhou with large area of high LST found in the downtown area in the northwestern part of the city. The temperature difference between the downtown and surrounding rural areas reaches up to 12 °C in LST. In particular, Hangzhou Bay in the southeast has a surface UHI intensity of 10 °C since it is an economic development zone surrounded by Hangzhou, Shanghai and Ningbo, leading to such the prominence of surface UHI in this area.

3.4. Relationships between LST and LCZ classes

Fig. 4 shows the differences of LST from the mean value for each LCZ class. In general, there are large variations in LST across LCZ classes while the pattern is similar between the two cities despite of the higher differences observed in Hangzhou. The LST of built-up LCZ classes is generally higher than that of the land cover classes, reiterating the high UHI intensity in urban areas. In particular, LCZ 1 (compact high-rise) has the highest LST among the built-up LCZ classes with mean values of 27.3 °C and 20.8 °C for Shanghai and Hangzhou respectively. LCZ 9 (sparsely built) shows opposite trend in the two cities with 0.2 °C above mean in Shanghai but 1.8 °C below mean in Hangzhou. The complex and diverse urban morphology of this LCZ class in YRD is the predominant reason for such an opposite trend since most of the LCZ 9 areas in Hangzhou are located in mountain areas and villages surrounded by farmland and forest. In contrast, LCZ 9 in Shanghai is generally found in suburbs which experienced rapid urbanization and extensive conversion of land cover.

Lower LST is generally observed in land cover LCZ classes due to the extensive pervious surface in natural land cover. LCZ A exhibits the lowest LST in both cities with mean values of 26.1 °C and 15.4 °C observed in Shanghai and Hangzhou respectively. However, there are certain inconsistencies in LST of land cover classes due to the temporal difference in vegetation. Above-mean values were observed in LCZ E (bare rock or paved) in which some of them are concrete paved areas like airport and scattered settlements. LCZ G has the highest LST due to the highest heat capacity, which cools off slower than other LCZ classes during night-time.

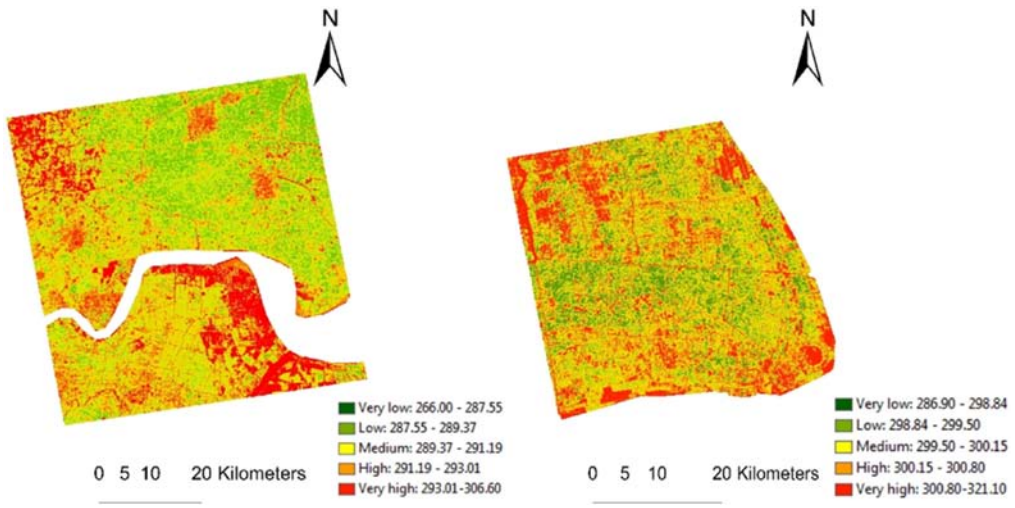

Fig. 3. Spatial variation of surface UHI in Hangzhou (left) and Shanghai (right).

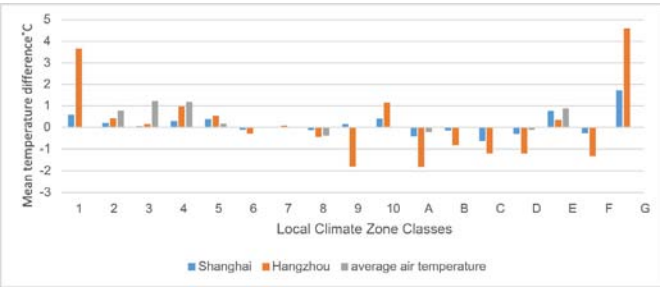

Fig. 4. Temperature differences (°C) from mean LST for each LCZ class.

After incorporating air temperature, it can be found that the existing 28 stations can represent 8 LCZ classes, namely LCZ 2, LCZ 3, LCZ4, LCZ 5, LCZ 8, LCZ A, LCZ D and LCZ E. Also, air temperature has the same variation of mean temperature difference with LST difference. The built -up LCZs except LCZ 8 are above the mean value while vegetation like LCZ D and LCZ E has lower air temperature. The similar variation trend confirms the traditional LCZ definition as well as the LST patterns of each LCZ.

4. Discussion

4.1. Representation of urban morphology of the YRD cities

4.1.1. Regional level

The LCZ maps produced by using the improved WUDAPT methodology were found to be representative for the urban morphology at both city and regional scales. The urban areas in the YRD megaregion can be classified into four urban agglomerations since the urban morphology is similar with no remarkable delineations among the cities within the agglomerations (Fig. 5). Region A is comprised of Shanghai municipality and the surrounding Kunshan in Suzhou and Nantong. The dominant land use in this area is urban and built-up areas with much commercial activity. The urban sprawl of the cities in the region has expanded beyond their administrative boundaries. It has the highest level of urbanization among the four regions and the urban areas are extremely concentrated and compacted, merging into a large spatial agglomeration. Region B is the Suzhou-Wuxi-Changzhou urban agglomeration to the west of Shanghai. The built-up areas in this region are mainly industrial and commercial. High level of urbanization is being experienced in this region and they are likely to develop into a megalopolis in the future.

On the other hand, Region C, located in the Hangzhou Bay including cities like Hangzhou, Shaoxing and Ningbo, have expanded closely to one another along the coast and contains most of the compact commercial areas. In the north of the YRD megaregion, Region D consists of Nanjing, Zhenjiang, and Yangzhou, with Nanjing as the centre of urban development. The urban area is relatively sparse and smaller than the previous three regions in terms of the size of the city. The urban sprawl of the cities in this region is relatively independent and has not spread together. Due to the rapid economic development in the YRD megaregion, these four regions are expected to merge and form a megalopolis in the future.

4.1.2. City level

Despite of the merging trend in the YRD megaregion, cities exhibit their own characteristics in urban morphology due to their corresponding rates and scenarios of urban development. In Shanghai municipality, LCZ 1 dominates since buildings, especially those in commercial areas, are high-rise and the urban areas are merging into larger metropolis. In contrast, newly developed districts such as Pudong and Baoshan are well-regulated with homogeneous urban morphology. Downtown areas like Changning district are more irregular in size and urban form since they are at the early stage of urban development.

Cities at sub-provincial level such as Nanjing and Hangzhou have less built-up areas than Shanghai municipality. High-rise buildings and CBDs are generally sparsely located in the city centre and often mixed with mid-rise buildings. The block size is usually around 300 m. For prefecture-level cities like Wuxi and Yangzhou, residential areas dominate and are mostly classified into LCZ 4 and 5. The blocks in these cities are relatively

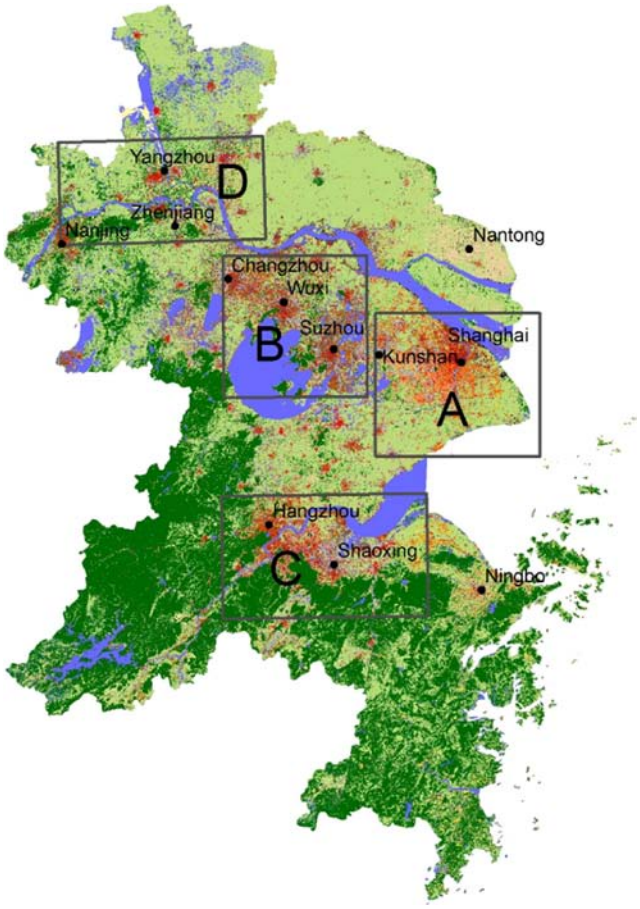

Fig. 5. Urban agglomerations identified in the YRD megaregion.

small and disperse with block size less than 100 m. The land use is highly mixed in these cities and the length of a land with homogeneous urban morphology is only around 70–80 m.

Small building blocks mixed with dominant LCZ classes cause problems in selecting training samples from Google Earth, which affect the accuracy of LCZ mapping using the WUDAPT method. In this study, it was found that training samples with size larger than 100 m^2 improved mapping results since they provide sufficient information for the classification. On the other hand, sample with area less than 100 m^2 cannot cover one pixel of the Landsat image so the chance of generating an erroneous classification is considerably increased. It is also likely to cause pixel mixing due to uncertainties about the location of different physical landscape. However, large samples of homogeneous urban morphology were absent in some cities like Wuxi, leading to poor mapping results when they were applied to satellite images of 100 m resolution. In order to improve the mapping result, the small samples and the original Landsat data of 30 m resolution were used for classification. Thus the Landsat data can better represent the spectral information of the samples and the classification accuracy has therefore been improved. Sub-classification of the mix LCZs types can also be helpful for improving the mapping result.

4.2. Implications for urban planning

As the LCZ classification scheme is based on the impact of urban morphology on temperature variation in the city, the LCZ maps are able to indicate the spatial distribution of the UHI phenomenon, which contribute to

more climate-sensitive urban planning. The LCZ map visualizes the spatial characteristics so urban planners and architects are able to better understand the thermal environment in the decision-making process. In addition, the LST characteristics of LCZ classes are helpful to minimize the impacts of urbanization by using urban vegetation and land use planning.

More severe UHI phenomenon was found in the central and southern parts of the YRD megaregion due to the higher level of urban development. Frequent communications between the cities in this part of the region facilitate the emergence of these cities into megalopolis. Therefore, more careful planning strategies are required for future urban development with respect to UHI mitigation. For the dense urban areas in Shanghai, Hangzhou and Nanjing, further urban development should be avoided or carefully designed in order to alleviate the high temperature. Green patches with low UHI intensity can also be strategically used to effectively mitigate UHI phenomenon. For areas with high UHI, it is also important to improve the thermal environment through measures such as efficient energy use, building materials and other ecological measures (Chen et al., 2016).

The urban areas of prefecture-level cities such as Wuxi and Suzhou are sparsely distributed. Hotspots of the cities have sprawled from city centre to urban fringe and suburban areas while local hotspots emerge in new towns where a large area of vegetation was converted to impervious surface cover. It suggests that urban development in these areas should be carefully planned and designed, for example, providing open space, preserving urban greenery and enhancing ventilation. These measures are able to provide cooling effect to mitigate the UHI intensity in these areas.

The extensive industrial zones in the YRD megaregion such as Baoshan district in Shanghai and Hangzhou Bay also exhibit high LST and worsen the thermal environment. Further measures should be considered to not only limit the building density, but also restrict the anthropogenic heat release of the industrial area. Natural land cover such as green space (LCZ A–D) and open space (LCZ E and F) are beneficial to the surrounding areas. Low building density is therefore preferred in order to maximize the cooling effect and prevent any blockage of ventilation from these areas.

4.3. Further work

This study provides information about urban morphology and potential UHI patterns and can thus help facilitate climate-sensitive urban planning and design. In response to global climate change, the National Climate Change Adaptation Plan (2004–2010) and National Ecological Protection and Construction Plan were proposed to mitigate the UHI phenomenon and improve the living quality of urban environment (National Development and Reform Commission, 2013, 2016). To facilitate these planning strategies, land use and urban morphological data are required, but access to these data is generally limited in China. LCZ maps therefore offer a freely available option for urban planners and urban climate researchers to acquire the necessary information for climate-sensitive planning.

Besides, the Chinese government highlights the importance of promoting ecological progress in the Thirteenth Five-Year Plan due to the shortage of resource and energy (Ministry of Environmental Protection of China, 2016). The construction of eco-cities has thus become the new direction and goal of China's urban development. Since 2012, 272 eco-cities have already been planned (Lin, 2013). The LCZ map can provide basic urban form data for eco-city evaluation. The evaluation criteria such as Ventilation Potential Index, urban heat island proportion index (UHPI) and Ecological cold area ratio (Ministry of Housing and Urban-Rural Development of China, 2015) are characterized by sky view factor, surface roughness, UHI intensity and NDVI, which can be well represented in the LCZ map.

In addition, the 100 m resolution LCZ information acquired by the improved WUDAPT can provide necessary information for urban planning and eco-city evaluation not only at mesoscale, but also local and microscale. These will be useful in developing planning strategies for the regional and city group plan, city master plan, community plan and building design to mitigate the UHI effects and ensure the well-being of the habitants of the country.

Furthermore, under future climate change, the frequency and duration of heat waves are expected to increase in China (Wang and Zheng, 2013). The understanding of potential UHI patterns can be adopted for risk management of heat wave events in the future. LCZ maps can also identify hot spots and potentially problematic areas that require attention in heat wave studies.

4.4. Limitations

The present study focuses on the LST and corresponding UHI patterns in summer. Seasonal variations in UHI patterns would help to understand the LST characteristics due to urban morphology more comprehensively. Multi-temporal satellite images are required to further investigate the relationship between LST and LCZ classes in different seasons. As the Landsat images do not provide satisfactory differentiation of land cover LCZ classes, NDVI can provide an alternative source of data for more accurate classification of vegetation covers. Stereo images can also be used to extract urban morphological parameters and hence improve the accuracy of classification of built-up LCZ classes. Besides, low-cost but more detailed satellite images can be used to replace Landsat images in the classification process (Ren et al., 2016a, 2016b). Moreover, the current air temperature records collected from available national weather observational stations can only represent 8 LCZ classes. More air temperature data such as local weather observational records are needed to gain a more comprehensive understanding of the temperature pattern of LCZ. In addition, many cities in the YRD region have mixed LCZ classes and small blocks that are less than 100 m^2. The existing LCZ classification scheme is not adequate to describe the surface features of these cities. Therefore, future efforts should be made to refine and localize the LCZ classification for Chinese cities.

5. Conclusion

The development of megaregions is a national strategy which focuses on future urban development in China. This study has adopted an improved WUDAPT method to develop a regional LCZ map for the YRD region with higher accuracy results of LCZ classification and efficiency in terms of time and man power cost. A single-channel method was used to acquire LST of Shanghai and Hangzhou from night-time Aster thermal data and UHI intensity was subsequently obtained based on LST. Furthermore, air temperature records of local ground observatory stations were collected and analyzed to get a more comprehensive findings and understanding on the potential UHI distribution pattern of LCZs.

Although the concept of LCZ classification scheme is based on measurements of air temperature, LST was found to be associated with LCZ classes, using the comparison between two YRD cities. Built-up LCZ classes generally exhibit higher LST than land cover LCZ classes. LCZ 1 and 10 have the highest LST among the built-up classes in the two cities while vegetation (LCZ A–D) has the lowest among all classes. Inconsistencies in LST variations were found in LCZ 9, A, B and C due to the highly variable urban morphology and the temporal variations in vegetation. The air temperature analysis also confirms the LST patterns of each LCZ.

Findings of the present study generally support the concept of LCZ and WUDAPT mapping method at both regional and city levels in the YRD megaregion, which agrees with previous studies (Geletič et al., 2016). They also help urban planners and urban climate researchers better understand the influence of urban morphology (i.e. LCZ classes) on local climatic conditions. Results also support climate-sensitive urban planning, eco-city evaluation and heatwave studies at regional and city levels. In addition, the LCZ maps can be used as input data for model simulation for climate change studies. More detailed remote sensing dataset can better capture the urban forms characteristics and can thus be used in the classification process to support model simulation at different resolution. Further studies are required to examine seasonal differences of LST, improve the quality of data and sub-classification of mixed LCZ classes.

Acknowledgement

The study is supported by The Vice-Chancellor's Discretionary Fund of The Chinese University of Hong Kong. It is also funded by a General Research Fund Project Grant 2016/17 (Project No.: RGC-GRF 14643816, named “A study of “Local Climate Zone (LCZ)” of Sub-tropical China's Pearl River Delta region by using the WUDAPT method for better comfortable living and sustainable urban planning”) of Hong Kong Research Grants Council. The authors are grateful to Dr. Ming Luo for providing air temperature data from national weather observational stations. The authors also wish to thank Prof. Gerald Mills, Dr. Jason Ching, Dr. Benjamin Bechtel for their valuable suggestions to this study.

References

Amekudzi, A.A., Banerjee, T., Barringer, J., Cmapbell, S., Contant, C.K., Doyle, J.L.H., Ankner, W., Fainstein, N., Fainstein, S.S., Faludi, A.K., Florida, R., 2012. Megaregions: Planning for Global Competitiveness. Island Press.

Bechtel, B., Alexander, P., Böhner, J., Ching, J., Conrad, O., Feddema, J., ... Stewart, I., 2015. Mapping local climate zones for a worldwide database of the form and function of cities. ISPRS Int. J. Geoinf. 4 (1):199–219. http://dx.doi.org/10.3390/ijgi4010199.

Cai, M., Ren, C., Xu, Y., Dai, W., Wang, X.M., 2016. Local climate zone study for sustainable megacities development by using improved WUDAPT methodology – a case study in Guangzhou. Procedia Environ. Sci. 36:82–89. http://dx.doi.org/10.1016/j.proenv.2016.09.017.

Chen, L., Jiang, R., Xiang, W.-N., 2016. Surface heat island in Shanghai and its relationship with urban development from 1989 to 2013. Adv. Meteorol. 2016:1–15. http://dx.doi.org/10.1155/2016/9782686.

Ding, J., Zhang, Z., Xi, H., 2014. A study of the high temperature distribution and the heat island effect in the summer of the Shanghai area. Chin. J. Atmos. Sci. 26 (3), 420–431 (Chinese edition).

Dong, L.-p., Jiang, Z.-h., Shen, S.-h., 2014. Urban heat island change and its relationship with urbanization of urban agglomerations in Yangtze River Delta in past decade. Trans. Atmos. Sci. 37 (2), 146–154.

ERSDAC. 2010. ASTER GDS, from http://www.gds.aster.ersdac.or.jp/gds_www2002/exhibition_e/a_sensor_e/set_a_sensor_e.html.

Geletič, J., Lehnert, M., Dobrovolný, P., 2016. Land surface temperature differences within local climate zones, based on two Central European cities. Remote Sens. 8 (10):788. http://dx.doi.org/10.3390/rs8100788.

Jiménez-Muñoz, J.C., 2003. A generalized single-channel method for retrieving land surface temperature from remote sensing data. J. Geophys. Res. 108 (D22). http://dx.doi.org/10.1029/2003jd003480.

Jiménez-Muñoz, J.C., Sobrino, J.A., Gillespie, A., Sabol, D., Gustafson, W.T., 2006. Improved land surface emissivities over agricultural areas using ASTER NDVI. Remote Sens. Environ. 103 (4):474–487. http://dx.doi.org/10.1016/j.rse.2006.04.012.

Liaw, A., Wiener, M., 2002. Classification and regression by randomForest. R News 2 (3), 18–22.

Lin, F., 2013. Discussion on China's Eco-city Planning.

Ministry of environmental protection of China, 2016. Outline of the Thirteen Five-Year Plan of National Ecological Protection.

Ministry of Housing and Urban-Rural Development of China, 2015. Guidance on Environmental Performance Evaluation of Urban Ecological Construction (for Trial Implementation).

National Bureau of Statistics of China, 2014. Statistical Communiqué of the People's Republic of China on the 2014 National Economic and Social Development Beijing, China.

National Development and Reform Commission, 2016. Regional Planning of Yangtze River Delta Beijing, China.

National Development and Reform Commission, 2013. China: National climate change adaptation plan. National Development and Reform Commission, 2016. National Ecological Protection and Construction Plan.

Nichol, J.E., To, P.H., 2012. Temporal characteristics of thermal satellite images for urban heat stress and heat island mapping. ISPRS J. Photogramm. Remote Sens. 74:153–162. http://dx.doi.org/10.1016/j.isprsjprs.2012.09.007.

Oke, T.R., 1982. The energetic basis of the urban heat island. Q. J. R. Meteorol. Soc. 108, 1–24.

Oke, T.R., 1987. Boundary-layer Climate. Routledge, London.

Ren, C., Cai, M., Wang, R., Xu, Y., Ng, E., 2016a. Local Climate Zone (LCZ) Classification by using the method of World Urban World Urban database and Access Portal Tools (WUDAPT): a case study in Wuhan and Hangzhou. Paper Presented at the Fourth International Conference on Countermeasure to Urban Heat Islands (4th IC2UHI). Singapore.

Ren, C., Liu, S.Y., Lee, A., Ho, J.C.K., Xu, Y., Lau, K., Wang, W.W., 2016b. Urban Ventilation Assessment and Wind Corridor Plan: Creating Breathing Cities. China Architecture &Building Press, Beijing, China.

Schrijvers, P.J.C., Jonker, H.J.J., Kenjeres, S., de Roode, S.R., 2015. Breakdown of the night time urban heat island energy budget. Build. Environ. 83, 50–64.

Shanghai Municipal Statistics Bureau, 2011. Shanghai Statistical Yearbook 2000–2011. China Statistics Press, Beijing.

Sobrino, J.A., Jiménez-Muñoz, J.C., 2010. A single-channel algorithm for land-surface temperature retrieval from ASTER data. IEEE Geosci. Remote Sens. Lett. 7 (1), 176–179.

Stewart, I.D., 2011. Redefining the Urban Heat Island. Doctoral dissertation. University of British Columbia.

Stewart, I.D., Oke, T.R., 2012. Local climate zones for urban temperature studies. Bull. Am. Meteorol. Soc. 93 (12):1879–1900. http://dx.doi.org/10.1175/bams-d-11-00019.1.

Stoll, M.J., Brazel, A.J., 1992. Surface-air temperature relationships in the urban environment of Phoenix, Arizona. Phys. Geogr. 13 (2), 160–179.

The state council of People's Republic of China, 2016. The 13th Five-Year Plan for Economic and Social Development of the People's Republic of China (the 13th Five-year Plan). Beijing, China.

Voogt, J.A., Oke, T.R., 2003. Thermal remote sensing of urban climates. Remote Sens. Environ. 86 (3):370–384. http://dx.doi.org/10.1016/s0034-4257(03)00079-8.

Wan, Z.J.D., 1996. A generalized split-window algorithm for retrieving land-surface temperature from space. IEEE Trans. Geosci. Remote Sens. 34 (4), 892–905.

Wang, C., Liu, J., 1982. The climate of the city of Hangzhou. Acta Geograph. Sin. 2 (37), 005.

Wang, W., Zheng, G., 2013. 2013 Green Book of Climate Change. Social Sciences and Academic Press.

Zhang, H., Qi, Z.-f., Ye, X.-y., Cai, Y.-b., Ma, W.-c., Chen, M.-n., 2013. Analysis of land use/land cover change, population shift, and their effects on spatiotemporal patterns of urban heat islands in metropolitan Shanghai, China. Appl. Geogr. 44:121–133. http://dx.doi.org/10.1016/j.apgeog.2013.07.021.

Zhu, Z., Woodcock, C.E., 2012. Object-based cloud and cloud shadow detection in Landsat imagery. Remote Sens. Environ. 118:83–94. http://dx.doi.org/10.1016/j.rse.2011.10.028.